Available online at www.sciencedirect.com
SCIENCE DIRECT®
ELSEVIER
Physica D 186 (2003) 109–132
PHYSICA D
www.elsevier.com/locate/physd

Wave attractors in a smooth convex enclosed geometry

A.M.M. Manders [a,*], J.J. Duistermaat [b], L.R.M. Maas [a]

[a] *Royal Netherlands Institute for Sea Research, P.O. Box 59, 1790 AB Texel, The Netherlands*
[b] *Department of Mathematics, Utrecht University, P.O. Box 80010, 3508 TA Utrecht, The Netherlands*

Received 14 January 2003; received in revised form 27 June 2003; accepted 10 July 2003
Communicated by A. Doelman

Abstract

The equations governing monochromatic internal or inertial waves in an enclosed two-dimensional basin lead in two dimensions to a hyperbolic equation in spatial dimensions. The wave rays have a fixed slope with respect to gravity or the rotation axis, depending on the frequency of the wave as compared to the strength of the stratification and the rotation rate of the fluid. This angle is conserved on the wave's reflection at the boundary. The slope of the rays is denoted by κ. Depending on κ and the geometry, either all wave rays are periodic (standing wave), no characteristic is periodic, or there is a limited number of periodic orbits to which wave rays are 'attracted'. In this study, the boundary is formed by the convex part of a third degree curve. Depending on a parameter ε, this curve varies between a circle ($\varepsilon = 0$) and a triangle ($\varepsilon = 2$), for $\varepsilon < 2$ it is completely smooth. The axis of symmetry (z-axis) is parallel to the direction of gravity/rotation axis, which are taken antiparallel. For the triangle and the circle the behaviour is well known: the corners of the triangle can attract wave rays, for the circle either all wave rays are periodic, or no wave ray is periodic, so that attractors do not exist. In the (κ, ε)-parameter space, investigation of the strength of convergence of characteristics yields Arnol'd tongues, stemming from $\varepsilon = 0$, broadening for increasing ε and finally all converging to $\kappa = \sqrt{3}$ for $\varepsilon = 2$. Tongues with attractors are bounded by values of κ for which wave rays either connect the top and bottom of the boundary or connect its critical points, where the wave ray is directly reflected back onto itself. As compared to nonsmooth geometries, corners are a degenerate form of critical points. Only for $\kappa = \sqrt{3}$ all wave rays return back onto themselves for all values of ε due to an additional symmetry, resulting in standing wave behaviour. If the symmetry of the curve with respect to the z-axis is removed by rotating it, the ordering of the periods of successive attractors changes and there is no standing wave mode. A general criterion, based on first order perturbation theory, is derived that states whether attractors exist for geometries that are small perturbations of the circle. For the geometry under consideration, first order perturbation theory is inconclusive and second order perturbation theory is used to verify the existence of the strongest attractor and to describe the Arnol'd tongue for small values of ε.
© 2003 Elsevier B.V. All rights reserved.

PACS: 47.35.+i; 47.54.+r; 92.10.Dh

Keywords: Internal waves; Gyroscopic waves; Pattern formation; Iterative maps

* Corresponding author. Tel.: +31-222-369412; fax: +31-222-319674.
E-mail address: manders@nioz.nl (A.M.M. Manders).

0167-2789/$ – see front matter © 2003 Elsevier B.V. All rights reserved.
doi:10.1016/j.physd.2003.07.003

1. Introduction

Stably stratified fluids can carry waves that travel obliquely through the fluid. For density-stratified fluids they are called internal waves, owing their existence to a balance between the pressure gradient force and buoyancy. For a uniformly rotating fluid they are called inertial or gyroscopic waves and the radial stratification in angular momentum provides elasticity to the fluid. For a rotating fluid that is also density-stratified these effects are combined into inertio-gravity waves. The rotation axis is taken antiparallel to the direction of gravity for convenience in this study, parallel to the z-axis. The slope of the wave rays depends solely on the wave frequency, the strength of the density stratification and the rotation rate and cannot be altered due to reflection. We will restrict ourselves to uniformly stratified, uniformly rotating fluids so that the wave energy travels along straight lines (wave rays).

If the basin, in which the fluid is contained, is uniform in one of the horizontal coordinates, it is justified to consider two-dimensional plane waves. The behaviour of monochromatic waves is then governed by a hyperbolic equation in spatial coordinates in the vertical plane [1,2]. For an enclosed basin, this is an ill-posed problem: solutions change dramatically when parameters are changed slightly. For some special basin geometries, like the circle or a rectangle, one is able to obtain 'classical' regular solutions in terms of eigenmodes (standing waves, seiches) where every wave ray reflects back onto itself. Examples can be found in [3] (circle, ellipse and rectangle), [4] (arbitrarily oriented ellipse) and [5] (rectangle and the half ellipse). When the shape of the geometry or the slope of the wave rays is changed infinitesimally the standing wave is destroyed.

In general, separation of variables is not possible and one must use the method of characteristics to solve the hyperbolic equation. The characteristics can also be interpreted as wave rays [5]. Because of the monochromatic Ansatz, time has been eliminated and the characteristics represent the spatial structure of the rays. It should be noted that a three-dimensional approach leads to a three-dimensional hyperbolic equation, called Poincaré equation [6], for which no such general method of solution is known to us for an enclosed basin.

When characteristics reflect at a sloping wall, they are focused or defocused. Reflection is not specular, parallel characteristics remain parallel. For internal waves propagating up a gentle slope, reflecting up-slope (subcritical reflection, horizontal component conserved upon reflection) at the slope and the surface, a decrease of wavelength and an increase of amplitude were predicted and observed in the laboratory [7,8]. For a triangle, characteristics approach one of the vertices. This is experimentally shown for inertial waves in a rotating cone [9,10], and described mathematically in [4]. In a different closed geometry, repeated reflection with focusing may lead to the approach to a limit cycle, the *wave attractor*. Examples are a basin of which the bottom is described by a parabola and a trapezoidal (bucket-shaped) basin [5], and the spherical shell [11].

For inertial waves the peculiarity of trapping of a wave (the existence of a closed orbit) for the spherical shell is known from the 1960s [12,13]. Closed ray paths were found for the equatorial region of a (thin) spherical shell. Somewhat later these trapped waves appeared to be limit cycles to which neighbouring wave rays converged [14,15], and it was noted that these limit cycles exist over continuous frequency intervals [16]. These limit cycles were later called wave attractors [5]. Solution of the hyperbolic equation on a closed domain can also be treated as a mapping of the circumference onto itself [17]. The mathematical notion of the existence of a limited number of periodic characteristics (attractors) for mappings of the circumference onto itself is older.

At first, a wave attractor was considered too pathological to be relevant for fluid dynamics [14]. Indeed, the mathematical attractor, with its infinitely large concentration of energy around it, cannot appear due to viscous and nonlinear effects. But the attractor may be a good first order approximation for patterns to occur in a fluid. In laboratory experiments, theoretically predicted attractors have been observed both for internal waves [18], and for inertial waves [19,20] in a basin with one sloping boundary. In numerical studies where viscosity was included, strong shear layers were found along patterns that were in agreement with the patterns of attractors predicted by

the inviscid limit, as long as the mathematical attractor did not reflect more than about 10 times at the boundary ([11,21] for the spherical shell).

The question arises what is essential for a geometry to bear the possibility of wave attractors. The spherical shell is a geometry with a 'hole' in the middle, it is not convex which introduces special behaviour due to the critical latitude singularity when the characteristic becomes tangent to the inner sphere [16,11]. In [5] the parabolic basin and a bucket were investigated. The parabolic basin showed the presence of attractors. The bucket was a hybrid geometry which showed both attractors and standing patterns, depending on the parameter values. Both geometries have corners, which can also play a special role since they act as critical points for all characteristics.

Here we study a geometry without such obvious special points. The smooth convex part of a third degree curve is adopted as a boundary. Depending on a parameter value, the convex part varies between a circle and a triangle. For the circle either all characteristics are periodic or no characteristic is periodic, for the triangle characteristics are always attracted to one of the corners. The behaviour of the characteristics is investigated in terms of a map of the boundary onto itself.

In the next section, the theory is explained and the map describing the successive reflections of a wave ray will be given. Also some definitions common in theory about one-dimensional maps are introduced. Then results will be shown from numerical iteration, followed by a discussion regarding the role of some special characteristics that close onto themselves. This leads to insight in the conditions under which attractors appear. Also, a criterion is derived that indicates whether attractors are present for first order perturbations to the circle. However, for the geometry under consideration second order theory is needed to describe the behaviour, as will be shown. Finally the results will be discussed and compared with results from literature.

2. Theory

We consider waves in an inviscid, linear, continuously stratified, steadily rotating Boussinesq fluid. The governing equations are the conservation of momentum, conservation of density and the continuity equation (see for example [22]). The time dependence is eliminated by assuming the waves to be monochromatic (frequency ω), resulting in a factor $\exp(-\mathrm{i}\omega t)$. The direction of gravity is the negative z-direction, the rotation axis is aligned along the z-axis. It is assumed that the basin is infinitely long in one horizontal direction, reducing the problem to a two-dimensional one. This enables the introduction of the stream function $\Psi(x, z)$ such that a single equation remains:

$$\frac{\partial^2 \Psi}{\partial x^2} - \kappa^2 \frac{\partial^2 \Psi}{\partial z^2} = 0, \tag{1}$$

with

$$\kappa^2 = \frac{\omega^2 - f^2}{N^2 - \omega^2}. \tag{2}$$

This is a wave equation (hyperbolic equation) in two spatial dimensions for real values of κ. N represents the buoyancy frequency, f the Coriolis parameter and equals 2Ω, with Ω the rotation frequency. The physical condition of no flow through the boundary requires that

$$\Psi = 0 \text{ at the boundary}. \tag{3}$$

We will construct solutions using characteristics, since the possibility of separation of variables is restricted to some specific boundary geometries. These characteristics describe the spatial pattern of wave rays (see [5] for discussion)

since time has been eliminated from the problem. The solution of (1) can be written in terms of the characteristic coordinates $\kappa x - z = c_1$ and $\kappa x + z = c_2$:

$$\Psi(x, y) = g(\kappa x - z) - h(\kappa x + z). \tag{4}$$

The slope of the characteristics is defined by κ, and as already mentioned solely depends on the wave frequency, the rotation rate and the buoyancy frequency. Therefore, these waves are sometimes called *monoclinical waves* [23]. In fluid dynamics, one often does not work with the slope of the characteristics but with the angle θ of the characteristics (wave rays) with respect to the direction of gravity or the rotation axis, which are always uniquely defined. Here $\theta = \pi/2 - \arctan\kappa$.

The functions g and h are functions of the two characteristic coordinates only. If they are prescribed on the boundary, the solution is determined. The values of g and h on the boundary are conserved along characteristics, and the values at the boundary determine the solution in the interior. But since the geometry is closed, characteristics are 'reflected' (like wave rays) and the functions g and h on the boundary must obey some periodicity condition to avoid incompatibility. However, on a fundamental interval (an interval between a point on the boundary from which a certain characteristic leaves and its nearest reflection point) the function can be prescribed arbitrarily. From a physical viewpoint, prescription of g and h replaces the prescription of a forcing mechanism. In order to satisfy $\Psi = 0$ on the boundary, the functional values of g and h are identical when restricted to incoming and outgoing characteristic at the same point, that is when characteristics belong to one web built by a certain characteristic and all of its reflections.

Propagating internal or inertial waves conserve their slope κ upon reflection. This is correctly represented by these characteristics. When two parallel characteristics reflect from a boundary that is parallel or perpendicular to the direction of gravity or the rotation axis, their distance is conserved. But when they reflect from a sloping boundary, their distance may decrease (focus) or increase (defocus). In an enclosed basin, when focusing is not balanced by defocusing, rays may ultimately end up in a limit cycle, the so-called attractor. The patterns arising from the reflections of the characteristics form the framework of the structure of the stream function.

We want to obtain solutions for Eq. (1) on the domain of which the boundary Γ is parameterized by the convex part of the third degree curve:

$$c = \frac{1}{\varepsilon}(x^2 + z^2) - z\left(x^2 - \frac{1}{3}z^2\right). \tag{5}$$

The parameter c is set to $c = (1/\varepsilon) - (1/3)$, to achieve that this curve is symmetric with respect to rotation over $(2/3)\pi$ around the origin. It has fixed points $(0, -1)$, $(-(1/2)\sqrt{3}, 1/2)$, $((1/2)\sqrt{3}, 1/2)$ regardless of the value of ε. The convex part varies between a triangle ($\varepsilon = 2$) and a circle ($\varepsilon \to 0$), depending on the value of the parameter ε. For $\varepsilon > 2$ there is no convex part, the curve then consists of isolated parts. The symmetry axes of the curve are the z-axis and the lines $z = \pm(\sqrt{3}/3)x$. Shapes of the curve for different values of ε are illustrated in Fig. 1.

The spatial structure of the wave field is determined by the pattern (web) formed by the spatial structure of the wave rays and their reflections. We will study the structure by describing the pattern formed by individual wave rays (characteristics).

A straight line has three intersection points with the third degree curve, one of these points lies outside the convex part. All three points are described by cubic roots. Expressions simplify if one of the intersection points is known, which is the case since one can choose a point on Γ as starting point for a characteristic. If the characteristic $z = \kappa x + b$ (belonging to the set of characteristics with positive slope) leaves from the point (x_n, z_n) on Γ, with $b = z_n - \kappa x_n$, then the next reflection point (x_{n+1}, z_{n+1}) is given by

$$z_{n+1} = \frac{1}{2z_n}\left(-z_n^2 - C_1 z_n \pm \sqrt{(z_n^2 + C_1 z_n)^2 + 4C_2 z_n}\right), \tag{6}$$

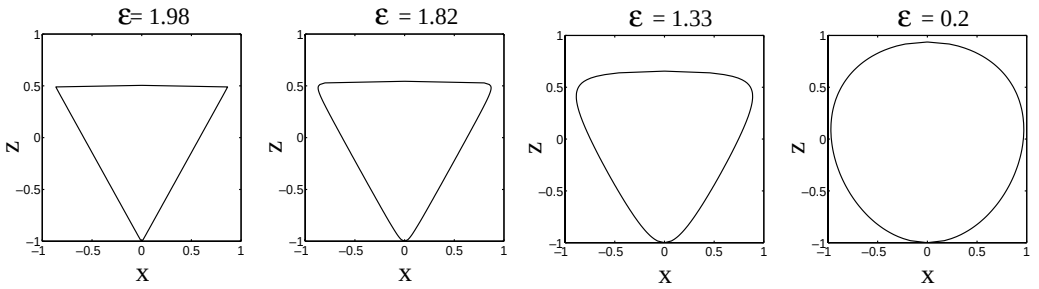

Fig. 1. Shape of the curve for different values of ε.

where

$$C_1 = \frac{-(1/\varepsilon)\kappa^2 - 2(z_n - \kappa x_n) - 1/\varepsilon}{1 - (1/3)\kappa^2}, \qquad C_2 = \frac{\kappa^2(1/\varepsilon - 1/3) - (1/\varepsilon)(z_n - \kappa x_n)^2}{1 - (1/3)\kappa^2}. \tag{7}$$

Now x_{n+1} follows from inserting z_{n+1} in the equation describing the characteristic, $x_{n+1} = (z_{n+1} - b)/\kappa$. The sign for the determination of z_{n+1} must be chosen as follows:

	$z_n < 0$	$z_n > 0$
$\kappa < \sqrt{3}$	+	−
$\kappa > \sqrt{3}$	−	+

(8)

For $z_n = 0$ the square root term vanishes, so there is no sign involved. The next iteration step is performed by following the same procedure, but now for the characteristic belonging to the set with slope $-\kappa$.

Following the successive reflections of a characteristics is equivalent to following the iterations of a map. Much is known about orientation preserving maps of the circumference to itself (see for example [24,25]). Therefore, an orientation preserving map is introduced, defined as the composition of two reflections, one for slope $+\kappa$ and one for slope $-\kappa$. Depending on whether one starts with characteristic with slope $-\kappa$ or with slope $+\kappa$ the map is said to be iterated forwards or backwards. This composite map will be called T and T^n is the nth iterate of the map. It maps Γ onto itself. The position of a point on Γ can be parameterized by a single periodic parameter ϕ, where $z = r(\phi)\cos(2\pi\phi)$, $x = r(\phi)\sin(2\pi\phi)$. The unusual convention of the coordinates is chosen in order to represent the symmetry in the z-axis. Here, for any integer k, the real numbers ϕ and $\phi + k$ represent the same point on Γ, we can make ϕ unique by restricting it to $[0, 1)$, but then have to jump discontinuously from 1 to 0 if we leave the interval at the right-hand boundary. The transformation T corresponds to a *continuous* transformation $\tilde{T}$, $R \to R$, which is unique up to addition of a constant integer k. If $\phi_0 \in [0, 1)$, then we can write $\tilde{T}^n(\phi_0) = \phi_n + m$, where $\phi_n \in [0, 1)$ and m is an integer, both uniquely determined. The ϕ_n are the representations in $[0, 1)$ of the iterates of T on Γ, and m can be interpreted as a winding number.

Different methods are used to study the behaviour of the 2-parameter map. Firstly, one can iterate the map for a certain parameter value combination (ε, κ) and directly plot a characteristic with its successive reflections. It gives a very intuitive insight in where focusing and defocusing take place on Γ.

Secondly, one can iterate the map for a range of values of one parameter, fixing the other parameter value. A Poincaré plot can be made by taking the last few hundred values of ϕ out of a larger number of iterations and repeat this for every parameter value. This plot gives insight in the change of behaviour of the map with the change of the parameter value regarding the presence and location of an attractor.

Thirdly, the rotation number can be computed. It measures the asymptotic average advance of ϕ per iteration of T. See for example [26] for details. The rotation number is defined as

$$\rho = \lim_{n\to\infty} \frac{\tilde{T}^n(\phi_0)}{n}. \tag{9}$$

If $\tilde{T}$ is replaced by $\tilde{T} + k$, where k is a constant integer, then ρ is replaced by $\rho + k$. This means that for the transformation $T : \Gamma \to \Gamma$ the rotation number is well-defined modulo integers. If the rotation number is rational, so that it can be expressed as $\rho = p/q$, p, q coprime, then there is a periodic orbit. The period of the orbit is q and $p < q$. If the rotation number is irrational, then the map is called quasiperiodic, the characteristics never close and finally fill a dense subset of the whole domain. The rotation number varies continuously and monotonously with the parameter value, and remains a constant, rational number in a window in parameter space for which there is a nondegenerate periodic point. A rational rotation number itself does not say anything about the character of a periodic orbit, it may be attracting or repelling (actually they usually occur in pairs, one attracting and one repelling) but it may also be neutral (every single ray is periodic, standing wave behaviour).

The Lyapunov exponent λ indicates whether a periodic orbit is an attractor, neutral or a repellor. The factor e^{λ} is the average factor with which a small interval $[\phi_0, \phi_0 + \epsilon]$ is stretched ($\lambda > 0$) or shrunk ($\lambda < 0$) after one iteration of the map. It is defined by (e.g. [27]):

$$\begin{aligned}\lambda(\phi_0) &= \lim_{N\to\infty} \lim_{\epsilon\to 0} \frac{1}{N} \log \left| \frac{T^N(\phi_0 + \epsilon) - T^N(\phi_0)}{\epsilon} \right| = \lim_{N\to\infty} \frac{1}{N} \log \left| \frac{\mathrm{d}T^N(\phi_0)}{\mathrm{d}\phi_0} \right| \\ &= \lim_{N\to\infty} \frac{1}{N} \sum_{n=1}^{N-1} \log \left| \frac{\mathrm{d}T(\phi_n)}{\mathrm{d}\phi_n} \right|. \end{aligned} \tag{10}$$

In this study, we will use an alternative formulation. We cannot work with the interval $[\phi, \phi + \epsilon]$ or the distance along the curve, since it depends on where the curve is intersected and therefore is not a measure of the convergence of the map. Therefore the perpendicular distance $\mathcal{D}$ between the characteristics passing through ϕ and $\phi + \epsilon$ is used. The ratio of the distance between rays before ($\mathcal{D}_{T^n}$)and after an iteration ($\mathcal{D}_{T^{n+1}}$) seems an appropriate measure from a physical viewpoint of focusing of a wave ray. We refer to the appendix for details for the derivation of λ in this specific case and just give the resulting formula:

$$\lambda(z_0) = \lim_{N\to\infty} \frac{1}{N} \sum_{n=1}^{N-1} \log \frac{\mathcal{D}_{T^n}}{\mathcal{D}_{T^{n-1}}}. \tag{11}$$

It should be noted that the *ratio* of distances has a meaning, individual distances cannot be eliminated.

For some basin shapes, it is possible to find a simple analytical expression for the Lyapunov exponent. An example is the bucket-shaped basin [5], a geometry with two sloping walls with constant slope. Since the slopes are constant and the map linear, λ can be determined with a 'bookkeeping' of the number of times that the ray reaches a divergent, convergent or neutral part of the map, corresponding to the sloping walls of the bucket or the horizontal walls. For the spherical shell, a very simple expression could be obtained for λ, in terms of the latitudes of the reflections [11].

In our case, it was not possible to derive a simple explicit analytical expression for the Lyapunov exponent, since the slope of the boundary, and therewith the strength of the focusing, varies with the 'latitude' (ϕ) in a more complicated way. As a check to the conventional method of considering a large number of reflections to study the limiting behaviour of the map for a random starting point, we could alternatively start directly on the attractor of period q itself and apply the map q times, and calculate the Lyapunov exponent from that. The results are still numerical approximations, but this method saves the averaging over the large number of iterations for a random

starting point. This method has been tested for the most simple attractor and the results agreed well with those for the conventional method.

3. Results

In this section, we will show results for different parameter values to study the dependence of the map on the parameters ε and κ.

To illustrate the geometry and the idea of focusing a picture of the fate of a characteristic for $\varepsilon = 1.82$ and $\kappa = 1.5$ is shown in Fig. 2(a). The corresponding stream function is also plotted. The characteristic starts to the right (forward iteration) and ends up in the limit cycle of period 2. This is the most simple attractor and it exists over a range of parameter values, although its exact location will change with changing parameter values. When we would have iterated the map backwards, the attractor would have been located at the left and would be a reflection of the former attractor in the z-axis. Depending on the direction of iteration and the exact starting point of a certain characteristic, one of the two is an attractor, the other a repellor. A characteristic may change its direction from going clockwise to anticlockwise when it reflects critically. Critical reflection means that the characteristic directly reflects back onto itself, which occurs when the tangent to the curve is equal to minus the slope of the characteristic. For this different circulation direction a former repelling limit cycle turns into an attractor.

There are three fundamental intervals where the function g (or h) in Eq. (4) can be prescribed: one in between the two z-symmetric limit cycles, one to the left and one to the right, all for $z > 0.5$ in this case. These intervals are shown as black lines at the top boundary, directly right from the middle and on the leftmost and rightmost side, in Fig. 2(b). All three intervals have their own domain of influence. This is illustrated in the stream function plot. The intense grey-tones appear where information of two different fundamental intervals is incorporated, the more modest tones indicate that the information comes from a single fundamental interval. In all three fundamental intervals a sine-function was prescribed, with different absolute values to illustrate the different domains of influence. The derivative of the sine-function is zero at the boundary of the interval, which guarantees smooth solutions except on the attractor. However, in practice the forcing mechanism for the waves is prescribed and the derivative at the end of

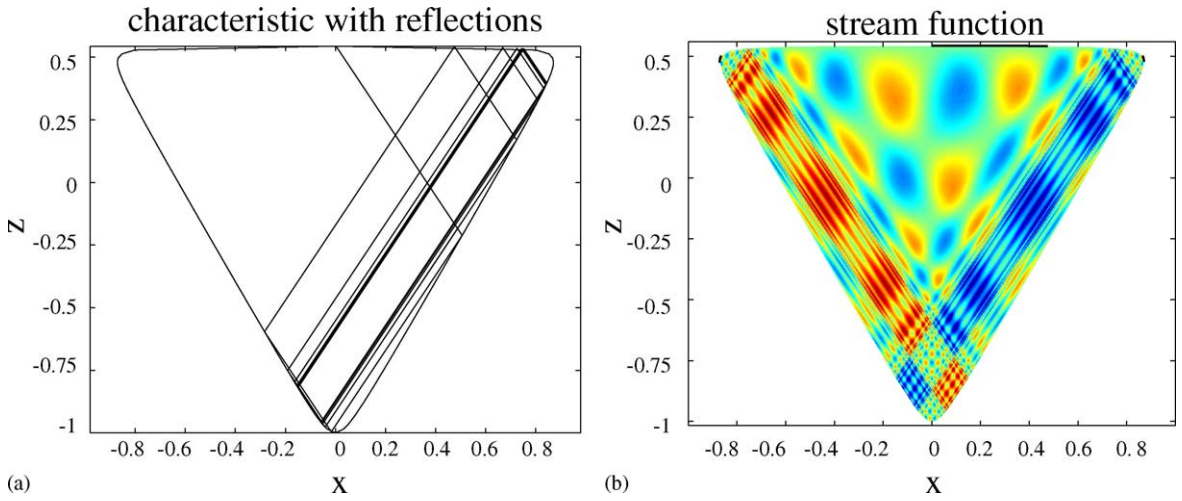

Fig. 2. (a) Characteristic approaching an attractor and (b) corresponding stream function for $\varepsilon = 1.82$ and $\kappa = 1.5$. The black lines at the boundary represent the fundamental intervals.

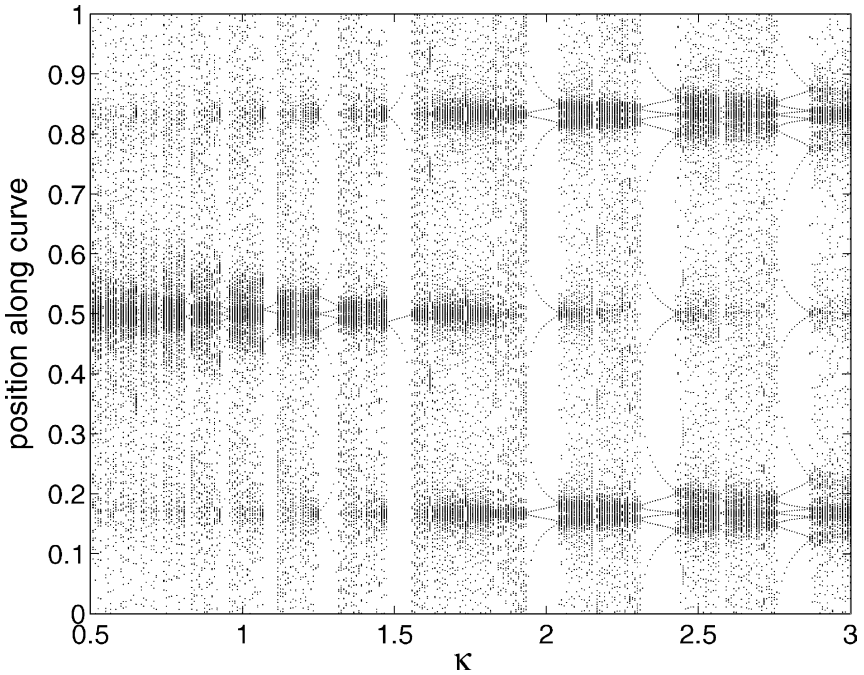

Fig. 3. Poincaré plot for $\varepsilon = 1.82$. Position on Γ of last 200 reflections out of 1000.

the fundamental interval is in general not smooth. Discontinuities in the velocity or the velocity gradient are reported for the precessing cylinder [28] and for forcing by oscillation of the end caps of a cylinder [29]. Mathematically, there are no objections. In physical experiments discontinuities in velocity or the velocity gradient have been observed [30].

In Fig. 3 the Poincaré plot is shown, where ε equals 1.82 and κ varies. There are distinct windows with attractors, separated by regions with high-periodic and quasiperiodic orbits. The regions with mostly quasiperiodic orbits may also contain attractors, but the intervals of κ over which they exist are too small to be visible on this scale. This will be illustrated later. Windows become substantially larger for increasing κ. This has the following simple reason. To investigate the whole range of slopes, κ should vary between 0 and ∞. The angle of the characteristic with respect to the direction of gravity or rotation axis θ only varies between $\pi/2$ and 0. With $\kappa = \tan(\pi/2 - \theta)$ the interval $\pi/4 \geq \theta \geq 0$ is smeared out over the region $1 \leq \kappa \leq \infty$, whereas the interval $\pi/2 \geq \theta \geq \pi/4$ is compressed in the interval $0 \leq \kappa \leq 1$. But since the parameter κ arises in the definition of the map and it gives a good resolution in the most interesting region we chose to use this parameter rather than work in terms of θ.

The rotation number and the Lyapunov exponent are shown in Fig. 4. The rotation number grows monotonously and remains constant in windows where a nondegenerate periodic point is present. The features of this graph, with a rapid increase of ρ just before and after an interval on which it is constant and many intervals in which ρ is constant, are also known as 'devil's staircase'. The Lyapunov exponent is nearly zero in the regions where the orbits are quasiperiodic or neutrally periodic and negative where the attractor exists. There is no interval on which $\lambda > 0$.

It is remarkable that in Fig. 3 in the interval $1.6 < \kappa < 1.9$ no window with attractor is detected. This coincides with a relatively rapid increase of ρ in Fig. 4(a). In this interval, the Lyapunov exponent (Fig. 4b) is nearly 0 and the minima of λ become less deep again for $\kappa > 1.9$. This behaviour is due to the presence of a standing wave mode (all characteristics reflect back onto themselves) for $\kappa = \sqrt{3}$. In Section 4, where more special orbits will be treated, we will see that the standing mode behaviour for $\kappa = \sqrt{3}$ occurs for all values of ε.

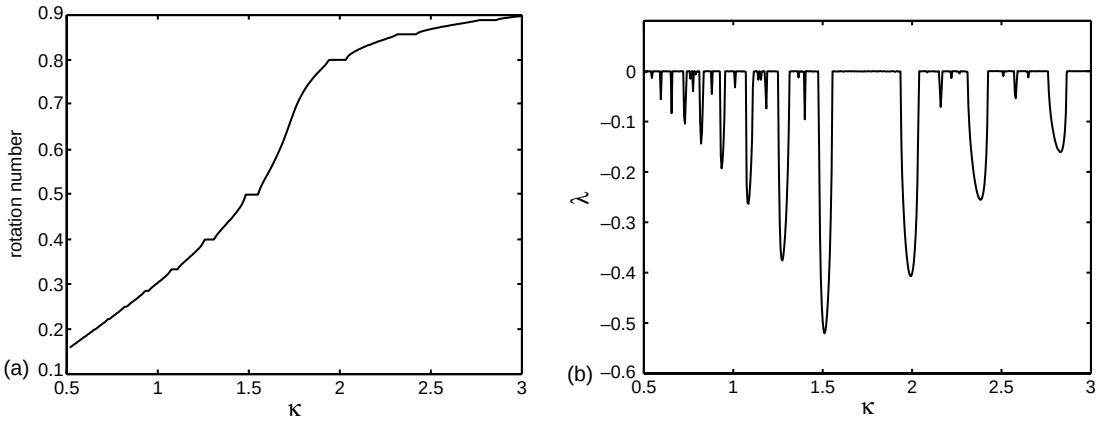

Fig. 4. (a) Rotation number and (b) Lyapunov exponent for $\varepsilon = 1.82$.

To compare and to investigate what the role of ε is we will also show results for other values of ε. We start with $\varepsilon = 1.98$, a parameter value for which the curve is close to a triangle. The plots of ρ and λ are in Fig. 5. As compared to the results for $\varepsilon = 1.82$ there are more and smaller intervals in which an attractor exists. The rotation number has a wider range for the same interval of κ-values. Also the negative peaks for the Lyapunov exponent are deeper and narrower. The interval around $\kappa = \sqrt{3}$, where no attractor is found numerically, is very small.

Fig. 6 shows results for $\varepsilon = 1.33$. In this case less attractor windows are visible than for $\varepsilon = 1.82$. The curve for the rotation number is monotonously increasing with just a few small intervals on which it is constant. Also the range of ρ is smaller than for $\varepsilon = 1.82$ on this scale, although for the full range of κ all values $0 < \rho < 1$ must be adopted. The structure of the Lyapunov exponent curve is very simple with just a few negative peaks. This is in sharp contrast with the abundance of structure for $\varepsilon = 1.98$. The depth of the peaks in κ for $\varepsilon = 1.98$ and $\varepsilon = 1.33$ differs by almost a factor 10. There is no attractor detected in a relatively wide range of κ around $\kappa = \sqrt{3}$.

The behaviour of the map is self-similar in the sense that when part of the plot is enlarged, it will show the same features as the 'original' plot, just on a different scale. This is illustrated in Fig. 7, where ρ and λ are plotted for all three values of ε. Especially for $\varepsilon = 1.98$ the self-similarity is clear. Between two relatively large scale attractors a

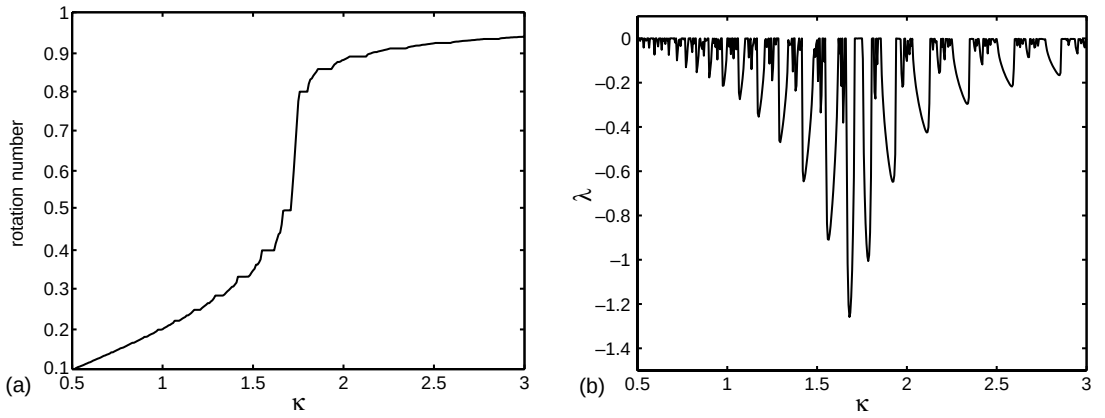

Fig. 5. (a) Rotation number and (b) Lyapunov exponent for $\varepsilon = 1.98$.

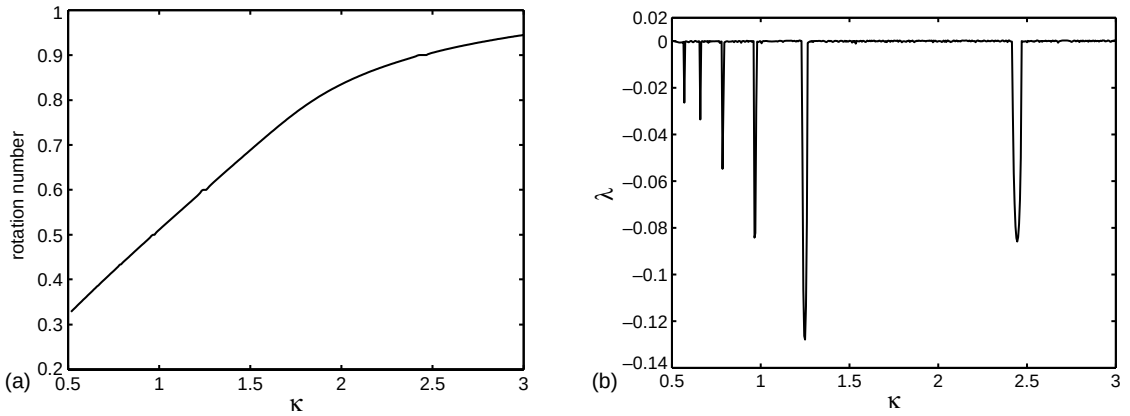

Fig. 6. (a) Rotation number and (b) Lyapunov exponent for $\varepsilon = 1.33$.

pattern arises that is similar to the original picture, with smaller and larger scale attractors, the Lyapunov exponent peaks becoming deeper and less deep again. If we enlarge part of the enlarged section we again find this structure. The structure of the enveloping line is reproduced also. On every scale we find patterns with the same structure. For $\varepsilon = 1.82$ the structure is also self-similar, but since the original picture did not show much structure in between the attractors we cannot expect different behaviour (much small scale structure). The structure for $\varepsilon = 1.33$ is very plain again. If we enlarge strongly we can also discern small negative peaks for λ in the interval around $\sqrt{3}$ where no attractor was visible in the original picture.

So far, the pattern of the dots in the Poincaré plot within a window with an attractor was continuous. We chose the starting point on the z-axis and the attractor shape was smoothly varying with the parameter value. However, if one chooses a random starting point (kept constant for the Poincaré plot), a discontinuity might arise in the Poincaré plot. An example is shown in Fig. 8. This occurs when the characteristics that are attracted towards one attractor are attracted to the mirror image of this former attractor for a slightly different value of κ. It happens very abruptly in parameter space and it can only occur for attractors that are not symmetric with respect to the z-axis themselves, but have a conjugate attractor that is its mirror image, like the period 2 attractor.

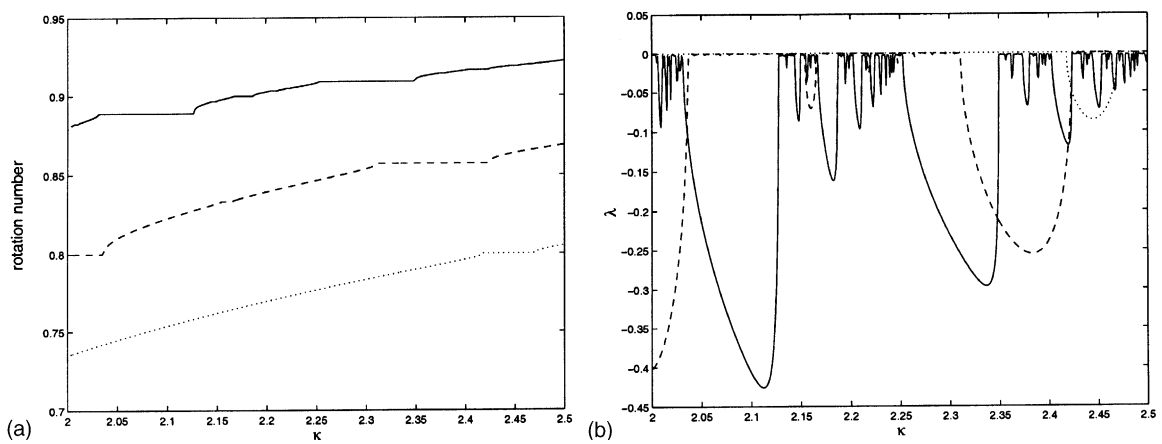

Fig. 7. (a) Rotation number and (b) Lyapunov exponent for $\varepsilon = 1.98$ (solid line), $\varepsilon = 1.82$ (dashed line) and $\varepsilon = 1.33$ (dotted).

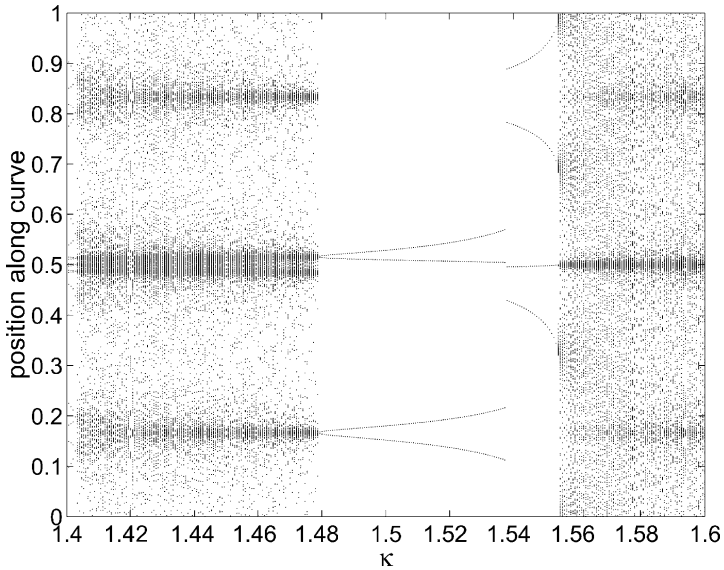

Fig. 8. Discontinuity in Poincaré plot for $\varepsilon = 1.82$, characteristics start at $z = -0.6$ instead of at $z = z_{\max}$ on the z-axis.

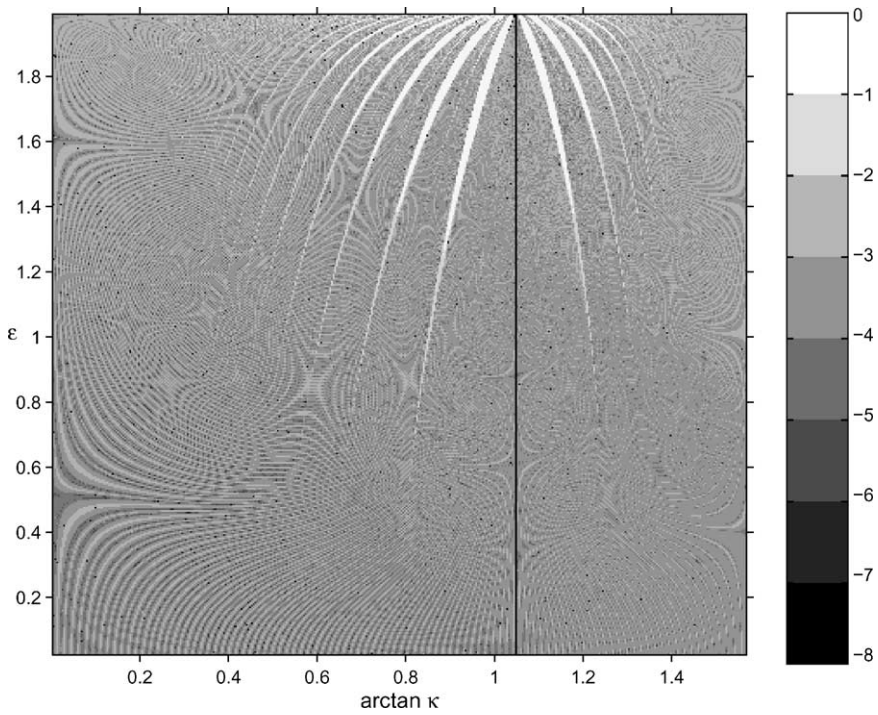

Fig. 9. Strength of convergence $\log_{10}(-\lambda)$ of characteristics for the whole parameter space.

To summarize the results and sweep through the complete parameter space a picture is made which shows the strength of convergence for all parameter combinations (Fig. 9). Instead of κ the angle $\pi/2-\theta = \arctan\kappa$ was used. This is done in order to show the whole parameter space. The strength of convergence is indicated by $\log_{10}(-\lambda)$. Regions of strong convergence can be beautifully recognized as broad 'tongues' at large values of ε, becoming very narrow at low values of ε and all bending towards $\arctan\kappa = \arctan\sqrt{3}$, which is the limiting value for all attractors at $\varepsilon = 2$. This is also the value for which the standing mode arises for all values of ε (black line). The tongue-like structures are called Arnol'd tongues, after [24]. Between the large scale tongues, corresponding to the major peaks in the Lyapunov exponent plots, there are smaller tongues corresponding to the smaller scale peaks. As stated earlier, because of the self-similarity of the structure for different scales, there must be an infinite number of smaller scale tongues. However, they are not resolved here, both because of the spatial scale of the plot and because the value of λ becomes very small. Outside the tongues there is an interference pattern, known as Moiré pattern. This is due to the finite resolution and not a feature of the map itself.

4. Special trajectories

As we have indicated before, a standing wave mode appears for $\kappa = \sqrt{3}$ for all values of ε. This can be explained by the symmetry of the curve, see Fig. 10. The curve has three axes of symmetry: the z-axis and the lines $z = \pm(1/\sqrt{3})x$. For $\kappa = \sqrt{3}$ all characteristics are orthogonal to the last two symmetry axes. The map can then be interpreted as a pure reflection in these two lines. For every single characteristic the boundary reflection points lie on a circle centred at the origin. There are two special orbits: one connecting the long axes of the curve (leading to the circle with largest diameter) and one connecting the short axes (leading to the circle with smallest diameter). These orbits connect the critical points. All characteristics intersect themselves on the z-axis.

There is an important difference in the behaviour of the characteristics for $\kappa < \sqrt{3}$ and $\kappa > \sqrt{3}$. For the triangle ($\varepsilon = 2$) we know that either the lower corner or the two upper corners act as attractor. For $\varepsilon < 2$ the curve has no real corners where the characteristics are trapped. But what we can observe is that for $\kappa < \sqrt{3}$ the characteristic reflects more often near the lower 'corner' whereas for $\kappa > \sqrt{3}$ the characteristic reflects more often in the two upper 'corners'. This is illustrated in Fig. 11 for two different period 5 attractors. The attractor for $\kappa < \sqrt{3}$ and

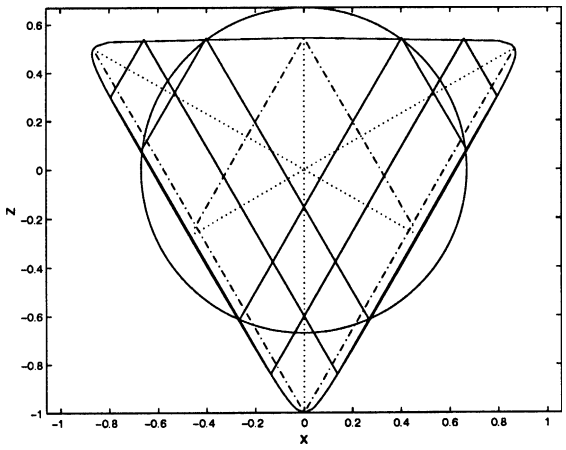

Fig. 10. Standing wave mode, $\kappa = \sqrt{3}$. The axes of symmetry are dotted, the special characteristics, connecting the critical points in pairs, are dash-dotted, solid lines are two arbitrary periodic characteristics. The circle, centred at the origin, connects the reflection points at the boundary of a single periodic characteristic. For every characteristic in this standing wave mode such a circle can be drawn.

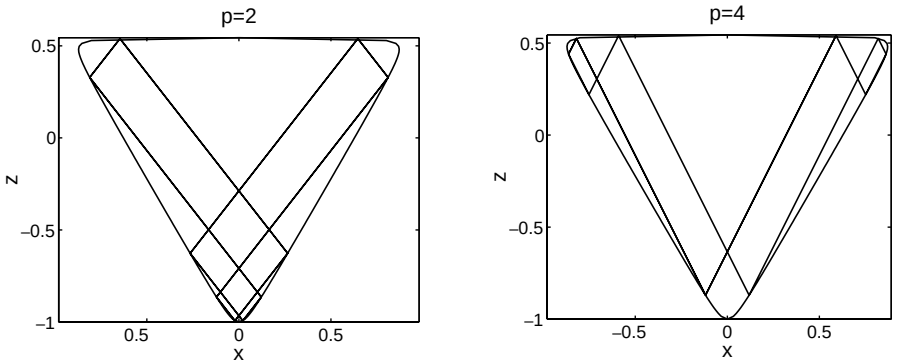

Fig. 11. Two attractors with the same period ($q = 5$) but a different location. For $\kappa = 1.28$, $p = 2$, reflection occurs mainly near lower 'corner', for $\kappa = 1.99$, $p = 4$, reflection occurs mainly near two upper 'corners'.

$p = 2$, $\rho = 2/5$ has more reflections near the lower 'corner', the one for $\kappa > \sqrt{3}$, $p = 4$, $\rho = 4/5$ has more reflections near the upper 'corners'. Both attractors correspond to large peaks of λ.

We also want to investigate the structure of the windows and the role of symmetric orbits and critical characteristics. In Fig. 12 the periods of the strongest attractors are indicated. Only the period 4 attractor for $\kappa > \sqrt{3}$ is not visible, as it is weak and its interval of existence is extremely small. In Table 1, the corresponding properties are indicated for increasing value of κ. Fig. 13 illustrates the paths of the characteristics at the boundary of the window for an odd and an even period window. It appears that windows with symmetric attractors (odd periods) are bounded by values of κ for which two (symmetric) critical points are mapped onto each other, on one boundary the upper, on the other boundary the lower. Windows with asymmetric attractors (even period) are bounded on one side by a value of κ for which two (asymmetric) critical points are mapped onto each other. On the other side, the two coexisting asymmetric attractors, that are each other's mirror image, merge into one single periodic orbit.

At the boundaries of the windows, there are no singularities or jumps in λ. It smoothly goes to zero, attraction is no longer exponential but algebraic. Because the two asymmetric attractors are attractors for opposed

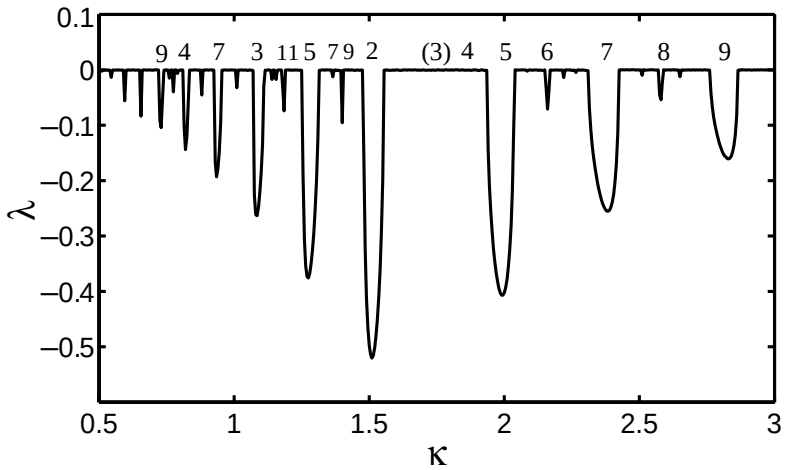

Fig. 12. Lyapunov exponent for $\varepsilon = 1.82$ with indication of the periods of the attractors and the standing wave.

Table 1
Typical properties of the strongest attractors regarding their symmetry and their structure at the beginning and end of their window of existence[a]

q	p	Symmetric	$\kappa_{\min}$	$\kappa_{\max}$
9	2	Yes	C–C	c–c
4	1	No	C–c	sym
7	2	Yes	C–C	c–c
3	1	No	C–c	sym
5	2	Yes	C–C	c–c
2	1	No	C–c	sym
3	2	–	–	–
4	3	No	sym	C–c
5	4	Yes	C–C	c–c
6	5	No	sym	C–c
7	6	Yes	C–C	c–c
8	7	No	sym	C–c

[a] c means that the periodic orbit starts and ends in critical points: C indicates a critical point in the upper part of the curve, c in the lower. If the end of the window consists of a symmetric attractor formed by the merging of two asymmetric attractors this is denoted by 'sym'.

sense of the map, it seems natural that attraction is cancelled when they merge. Similar behaviour was observed for the spherical shell [11], when the attractor reflects at the inner sphere at the equator. This also corresponded to the merging of two coexisting attractors that are each other's mirror images with respect to the equator.

Table 1 and Fig. 12 also illustrate the difference in the ordering of the windows for κ larger and smaller than $\sqrt{3}$. The properties of the attractors are in a sense symmetric around $\kappa = \sqrt{3}$. But the ordering of the periods of the windows is different. For $\kappa < \sqrt{3}$ the periods of the largest windows, starting from the large period 2 windows, are $2, 5, 3, 7, 4, 9, \ldots$. For $\kappa > \sqrt{3}$, it is a continuously increasing series with the odd periods for the large windows and the even periods for the smaller windows.

Smaller peaks in between the large peaks in Fig. 12 correspond to attractors of rather low period, but higher than the adjacent large windows (for example the period 9 and 7 attractors in between the period 2 and the period 5 attractor). The characteristics have a more complex reflection pattern than the characteristics that belong to the large windows. The even smaller peaks have intermediate period like 25 at $\kappa = 2.648$. But again these smaller windows are bounded by characteristics connecting the critical points or forming a symmetric orbit.

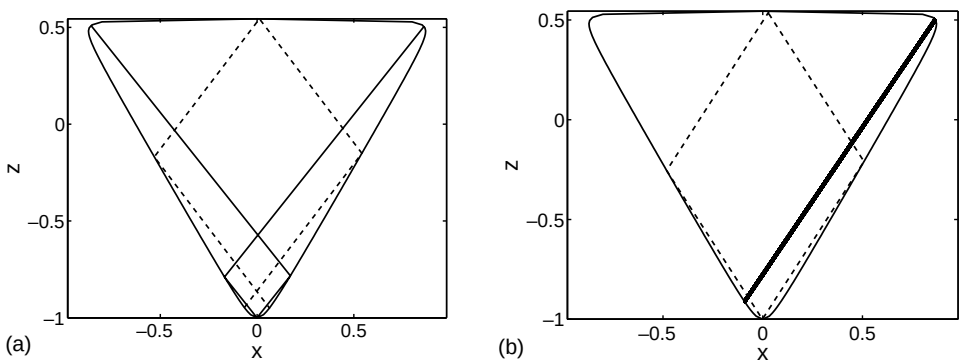

Fig. 13. Periodic characteristics that determine the boundary of a window: solid characteristics belong to the beginning of the window, dashed characteristics to the end of the window; (a) period 5 window ($p = 2$) and (b) period 2 window.

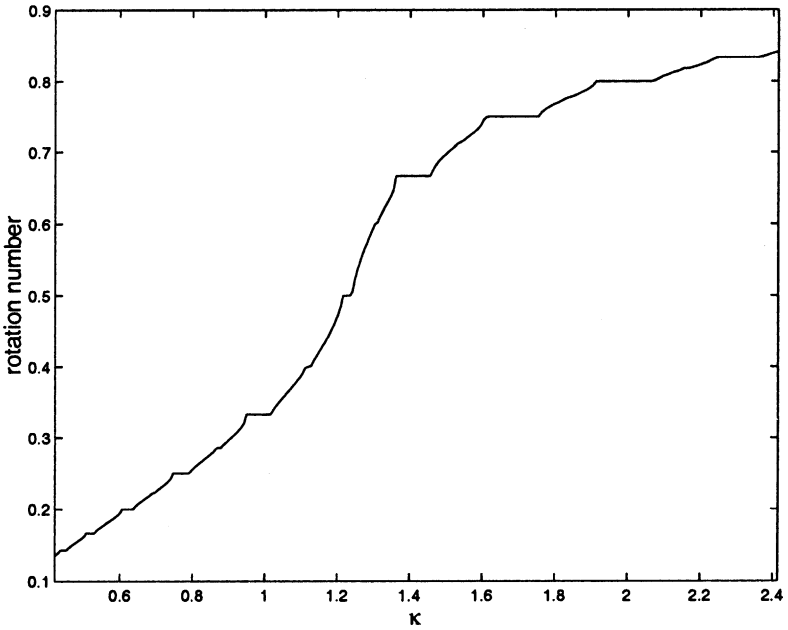

Fig. 14. Rotation number for $\varepsilon = 1.82$, curve rotated over 0.15 rad.

5. Breaking of basin symmetry

We investigated the role of symmetry breaking with respect to the z-axis. This was effectively done by rotating the curve around the origin by 0.15 rad. The angle of rotation was chosen such that it is not a rational fraction of 2π, but apart from this the exact value is rather arbitrary. The characteristics remain symmetric with respect to the vertical axis. The rotation number is plotted in Fig. 14. The strength of convergence over the whole parameter space is shown in Fig. 15.

The results look similar to the results with symmetry. The most striking difference is the absence of the standing wave mode. When we look in more detail and inspect the plot of the rotation number, we also note that the ordering of the periods of the attractors is different. With the period 2 window somewhere in the middle of the parameter space again, the major windows are more or less symmetric around the period 2 window, with a sequence of periods $3, 4, 5, 6, \ldots$ in both directions. Like in the case with symmetry, the critical points play an important role in defining the beginning and end of a window in parameter space. The windows with attractors with even period begin and end where critical points with the same tangent slope are mapped onto each other. The windows with odd period attractors begin and end where critical points with different tangent slope are mapped onto each other.

6. Perturbed circle

In this section, we consider the dynamics of a composition of two reflections for a general perturbation of the circle. A criterion is derived that states if attractors are present or not at first order of the perturbation.

For the circle, the composition of two reflections is a rotation. Consider the circle with radius equal to 1. The coordinate on the boundary is represented by α, with $0 \leq \alpha < 1$. The characteristics reflect in lines that make

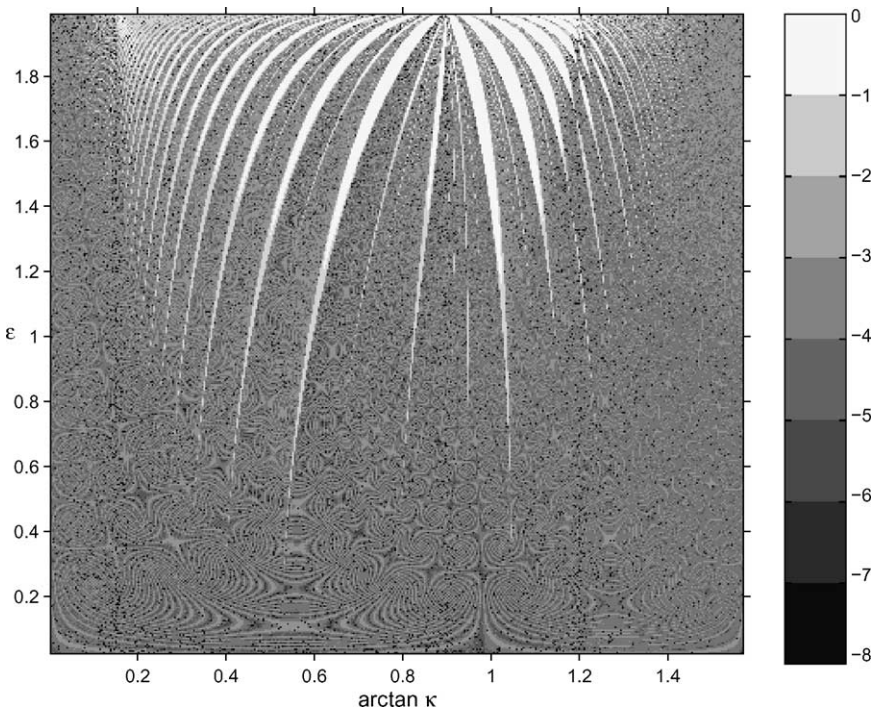

Fig. 15. Strength of convergence of characteristics over whole parameter space. The curve is rotated over 0.15 rad to break the original axial symmetry.

an angle ξ and θ with the horizontal axis. The situation is illustrated in Fig. 16. The involution with respect to ξ, denoted by $i_\xi(\alpha)$, maps α into $\beta = 2\xi - \alpha$ and $i_\theta(\alpha) = 2\theta - \alpha$. The composition $i_\theta(i_\xi(\alpha))$ yields $2(\theta - \xi) + \alpha$. The dynamics of the map is either periodic ($(\theta - \xi)/\pi = p/q$, period q) or quasiperiodic ($(\theta - \xi)/\pi$ irrational).

Now we consider the perturbed circle parameterized by $(r_\varepsilon(\alpha)\cos(2\pi\alpha), r_\varepsilon(\alpha)\sin(2\pi\alpha))$, where $r_\varepsilon(\alpha) = 1 + \varepsilon r_1(\alpha) + \cdots$ is a prescribed perturbation to the unit circle. The effect of a perturbation on a single reflection is

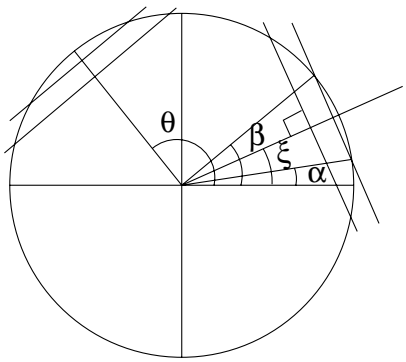

Fig. 16. Illustration of composition of two reflections for the circle. Reflection of characteristics in lines that make an angle ξ and θ with the positive horizontal axis.

investigated first. We denote $i_{\varepsilon,\xi}(\alpha)$ by β and expand:

$$\beta = i_{\varepsilon,\xi}(\alpha) = i_{0,\xi}(\alpha) + \varepsilon \left.\frac{\partial}{\partial\varepsilon} i_{\varepsilon,\xi}(\alpha)\right|_{\varepsilon=0} + \cdots \approx 2\xi - \alpha + \varepsilon\beta_1. \tag{12}$$

An extra index ε was introduced to i to discern the perturbed and unperturbed case. The first order term β_1 can be calculated as follows. Reflection in the line $z = \tan(\xi)x$ implies that β must satisfy

$$r_\varepsilon(\alpha)\cos(2\pi(\xi - \alpha)) = r_\varepsilon(\beta)\cos(2\pi(\beta - \xi)), \tag{13}$$

which relates the projections of $z = \tan(\alpha)x$ and $z = \tan(\beta)x$ on this line. The expansion (12) is substituted and both sides are differentiated with respect to ε in $\varepsilon = 0$. With the definition

$$\sigma_1(\alpha) = \left.\frac{\partial r_\varepsilon(\alpha)}{\partial\varepsilon}\right|_{\varepsilon=0},$$

the expression for β_1 is given by

$$\beta_1 = \frac{\sigma_1(2\xi - \alpha) - \sigma_1(\alpha)}{2\pi\sin((\xi - \alpha)2\pi)}\cos(2\pi(\xi - \alpha)). \tag{14}$$

With this result we can proceed to consider the composition of two reflections. To simplify things without loss of generality, ξ is set equal to 0 so that $i_{0,\xi}(\alpha) = i_{0,0}(\alpha) = -\alpha$. The orientation preserving map is defined by $T_{\varepsilon,\theta}(\alpha) = i_{\varepsilon,\theta}(i_{\varepsilon,0}(\alpha))$. We consider the composition $T^q(\alpha)$:

$$T_{\varepsilon,\theta}(\alpha) = \alpha + 2\theta + \varepsilon \left.\frac{\partial T(\alpha)}{\partial\varepsilon}\right|_{\varepsilon=0} + \mathrm{O}(\varepsilon^2), \tag{15}$$

$$T^q_{\varepsilon,\theta}(\alpha) = \alpha + 2q\theta + \varepsilon \left.\frac{\partial T^q(\alpha)}{\partial\varepsilon}\right|_{\varepsilon=0} + \mathrm{O}(\varepsilon^2). \tag{16}$$

We choose $2\theta = p/q$ so that $T^q_{0,\theta}(\alpha) = \alpha$, the identity, and p and q must have no common factors, $q > p$. We define $\tau_{1,\theta}(\alpha) = (\partial T(\alpha)/\partial\varepsilon)|_{\varepsilon=0}$. It can be calculated using the expressions for β_1:

$$\tau_{1,\theta}(\alpha) = \beta_{1,\theta}(-\alpha) - \beta_{1,0}(\alpha), \tag{17}$$

$$\tau_{1,\theta}(\alpha) = \frac{\sigma_1(2\theta + \alpha) - \sigma_1(-\alpha)}{2\pi\sin((\theta + \alpha)2\pi)}\cos(2\pi(\theta + \alpha)) + \frac{\sigma_1(-\alpha) - \sigma_1(\alpha)}{2\pi\sin(\alpha 2\pi)}\cos(2\pi\alpha). \tag{18}$$

We further can use that $T^j_{0,\theta} = \alpha + jp/q$ and $\partial T_{0,\theta}/\partial\alpha = 1$. This gives

$$\left.\frac{\partial T^q}{\partial\varepsilon}\right|_{\varepsilon=0} = \tau_1\left(\alpha + \frac{(q-1)p}{q}\right) + \tau_1\left(\alpha + \frac{(q-2)p}{q}\right) + \cdots + \tau_1(\alpha), \tag{19}$$

$$\left.\frac{\partial T^q}{\partial\varepsilon}\right|_{\varepsilon=0} = \sum_{j=0}^{q-1} \tau_1\left(\alpha + j\frac{p}{q}\right). \tag{20}$$

We have to determine $(\partial T^q/\partial\varepsilon)|_{\varepsilon=0}$ $(=\tau^q_{1,\theta}(\alpha))$ for a general form of the first order perturbation to the unit circle $\sigma_1(\alpha)$. Because $\sigma_1(\alpha)$ is periodic of period 1, it can be expressed as a Fourier series:

$$\sigma_1(\alpha) = a_0 + \sum_{k=1}^{\infty} a_k\cos(2\pi k\alpha) + \sum_{k=1}^{\infty} b_k\sin(2\pi k\alpha).$$

Then the expression for $\tau^q_{1,\theta}(\alpha)$ becomes, after a long but straightforward calculation in which the complex representation of a Fourier series was used:

$$\tau^q_{1,\theta}(\alpha) = \frac{q}{\pi}\sum_{l\geq 1}\left\{b_{2l}\left(\cos\left(2\pi l\frac{p}{q}\right)-1\right)+a_{2l}\sin\left(2\pi l\frac{p}{q}\right)\right\} - \frac{2q}{\pi}\sum_{m=1}^{\infty}\sum_{l\geq 1}\left\{b_{2l+mq}\left(\cos\left(2\pi l\frac{p}{q}\right)-1\right)+a_{2l+mq}\sin\left(2\pi l\frac{p}{q}\right)\right\}\cos(2\pi mq\alpha). \tag{21}$$

If $T^q_{\varepsilon,\theta}(\alpha)=\alpha$ has solutions for a finite number of values α, then there are attractors (or repellors) for these values of α. Since we explicitly chose θ such that $T^q_{0,\theta}(\alpha)=\alpha$, we can state that there are attractors (or repellors) if $\tau^q_{1,\theta}(\alpha)=0$ for a finite number of values α.

However, if $\tau^q_{1,\theta}(\alpha)=0$ holds for all values of α the theory is inconclusive. This holds for example for curves of which $\sigma_1(\alpha)$ does not contain Fourier coefficients of period 4 or higher. In such case, Arnol'd tongues may narrow stronger than linearly in ε (as is the case in [24]) and it is necessary to extend the analysis to a higher order. Alternatively the solution can be a standing mode. This notion puts a limitation to the practical value of the theory. But the theory clearly shows that for a variety of smooth geometries of a basin, attractors are possible, even with a tongue opening linearly in ε. Therefore the effect of corners turns out not to be crucial.

6.1. Application to ellipse and third degree curve

For the ellipse the radius r can be expressed as

$$r_\varepsilon(\alpha)=\sqrt{1-\varepsilon\sin^2 2\pi\alpha}, \tag{22}$$

$$r_\varepsilon(\alpha)\approx 1-\varepsilon\tfrac{1}{4}(1-\cos 4\pi\alpha), \tag{23}$$

with ε equal to the squared eccentricity. This yields nonzero Fourier coefficients a_0 and a_2 only and τ^q_θ equals zero. So there is not a finite number of solutions for α for which τ^q_θ=0. This correctly represents the fact that the ellipse does not allow for wave attractors [4]; either all characteristics are periodic or no characteristic is periodic. Therefore, higher order terms in the perturbation series would yield zero also. In fact the ellipse is equivalent to the circle, there is a linear transformation that maps the ellipse to the circle and the parallel characteristics get a slightly different orientation but remain parallel.

Eq. (21) is also applied to the third degree curve. For the third degree curve the radius of the convex part follows from:

$$1-\tfrac{1}{3}\varepsilon = r^2-\varepsilon r^3(\sin(2\pi\alpha)\cos^2(2\pi\alpha)-\tfrac{1}{3}\sin^3(2\pi\alpha)). \tag{24}$$

This results in the approximation:

$$r(\alpha)\approx 1+\varepsilon(-\tfrac{1}{6}+\tfrac{1}{6}\sin 6\pi\alpha), \tag{25}$$

which has the nonzero Fourier coefficients a_0 and b_3 for $\sigma_1(\alpha)$. This gives $\tau^q_\theta=0$ also. From closer inspection of (21) it follows that $\sigma_1(\alpha)$ must contain at least period 4 terms (a_4 or b_4 unequal to zero) in its Fourier expansion. If not, τ^q_θ does not depend on α. If we directly take characteristics parallel to the x- and z-axis, we find a standing mode of period 2 due to the symmetry of the curve in the z-axis.

Still we know from the previous results that attractors are indeed present. Fig. 9 suggests that these tongues are not a first order effect but must be sought in higher order. To avoid elaborate general second order analysis we

restrict ourselves to second order analysis of the period two attractor. Also, it is necessary to rescale and reorientate the curve in order to fit the curve in the conventions of this theory.

First we derive the expression for $\partial^2 T^2_{\varepsilon,\theta}(\alpha)/\partial\varepsilon^2|_{\varepsilon=0}$, which will be denoted by $\tau^2_{2,\theta}(\alpha)$ for convenience. The expression for β (Eq. (12)) can be extended with the next term in the Taylor expansion, $\beta \approx 2\xi - \alpha + \varepsilon\beta_1 + \varepsilon^2\beta_2$, with

$$\beta_2 = \left.\frac{\partial^2 i_{\varepsilon,\xi}(\alpha)}{\partial\varepsilon^2}\right|_{\varepsilon=0}.$$

In order to determine β_2 expression (13) must be differentiated twice with respect to ε and evaluated in $\varepsilon = 0$. With the definition

$$\sigma_2(\alpha) = \left.\frac{\partial^2 r_\varepsilon(\alpha)}{\partial\varepsilon^2}\right|_{\varepsilon=0}$$

this yields

$$\beta_2 = \frac{1}{4\pi \sin 2\pi(\xi-\alpha)}\left(\sigma_2(2\xi-\alpha) - \sigma_2(\alpha) - 4\pi^2\beta_1^2 + 2\beta_1 \left.\frac{\partial\sigma_1(\alpha)}{\partial\alpha}\right|_{2\xi-\alpha}\right)\cos 2\pi(\xi-\alpha) - \beta_1\sigma_1(2\xi-\alpha). \quad (26)$$

The term $\tau^2_{2,\theta}(\alpha)$ can be determined by straightforward differentiation of $i_{\varepsilon,\theta}(i_{\varepsilon,0}(i_{\varepsilon,\theta}(i_{\varepsilon,0}(\alpha))))$. Using the expressions for β_1, β_2 and $\tau_{1,\theta}(\alpha)$, this can be expressed as

$$\begin{aligned}\tau^2_{2,\theta}(\alpha) = {} & \beta_{2,\theta}(-2\theta-\alpha) - \beta_{2,0}(2\theta+\alpha) + 2\beta_{1,0}(2\theta+\alpha)\left.\frac{\partial\beta_{1,\theta}(\alpha)}{\partial\alpha}\right|_{-2\theta-\alpha} + 2\tau_{1,\theta}(\alpha)\left.\frac{\partial\tau_{1,\theta}(\alpha)}{\partial\alpha}\right|_{2\theta+\alpha} \\ & + \beta_{2,\theta}(-\alpha) - \beta_{2,0}(\alpha) + 2\beta_{1,0}(\alpha)\left.\frac{\partial\beta_{1,\theta}(\alpha)}{\partial\alpha}\right|_{-\alpha}. \end{aligned} \quad (27)$$

For the circle, in the above notation with $\xi = 0$, the angle θ is 1/4 and the characteristics are parallel to the x- and z-axis. The problem of the third degree curve was however consequently put in terms of two characteristics with opposed slopes, and only in the limit for small ε the characteristics belonging to the period two attractor become orthogonal. In order to use the first order analysis and extend it to a second order analysis we have to translate our problem to the appropriate coordinate system with one reflection in $\xi = 0$ and one in $\theta = 1/4$.

In the limit case $\varepsilon = 0$ the characteristics, belonging to period two, have $\kappa = \pm 1$ and are perpendicular. The curve only needs to be rotated over $\pi/4$ to be in the right coordinate system. However, as soon as $\varepsilon > 0$ the tongue bends away from $\kappa = 1$. In order to have perpendicular characteristics for the period two attractor we rescale the curve by replacing x by $(1 - C\varepsilon^2)x$. The values of C for which the tongue is found will follow from the analysis. Polar coordinates are introduced and the curve can be rotated over $\pi/4$. This results in the expression:

$$\begin{aligned} r_\varepsilon(\alpha) = {} & 1 + \varepsilon(-\tfrac{1}{6} - \tfrac{1}{12}\sqrt{2}(\cos 6\pi\alpha + \sin 6\pi\alpha)) + \varepsilon^2\tfrac{1}{144}(3 + 72C + 72C\sin 4\pi\alpha \\ & + 4\sqrt{2}(\cos 6\pi\alpha + \sin 6\pi\alpha) + 5\sin 12\pi\alpha) + \mathrm{O}(\varepsilon^3). \end{aligned} \quad (28)$$

Substituting this expression in Eq. (27) yields a periodic function for $\tau^2_{2,\theta}(\alpha)$. In Fig. 17(a) this function is plotted for $C = 0.2$. It has eight zeros for approximately the interval $0.06 < C < 0.3$, representing the two periodic orbits (attractors). For $C < 0.06$ the function is completely positive, for $C > 0.3$ completely negative. So we found the boundaries of the Arnol'd tongue belonging to the period two attractor to be $\kappa \approx 1 + 0.06\varepsilon^2$ and $\kappa \approx 1 + 0.3\varepsilon^2$. In Fig. 17(b), the boundaries of the Arnol'd tongue are plotted together with results representing parameter values

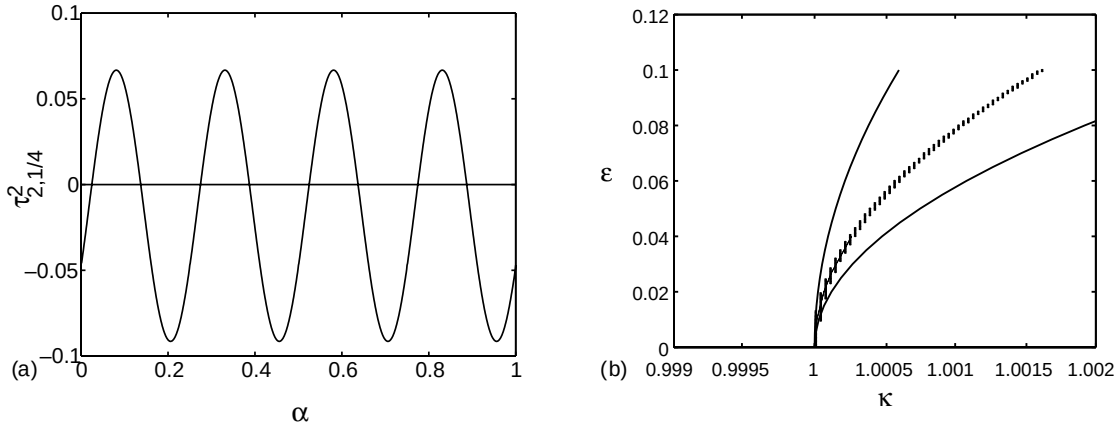

Fig. 17. (a) $\tau^2_{2,1/4}(\alpha)$ for $C = 0.2$. The eight zeros of the function correspond to the values of α on the two attractors. (b) Arnol'd tongue, bounded by $\kappa = 1 + 0.06\varepsilon^2$ and $\kappa = 1 + 0.3\varepsilon^2$. The vertical stripes indicate values for which convergence to a period 2 orbit was detected numerically.

for which numerical convergence to a period 2 periodic orbit was reached. It can be compared with Fig. 9 around $\arctan\kappa = \pi/4$. Apparently the tongue, as described by the second order perturbation theory, is subject to narrowing for $\varepsilon > 0.02$. This was confirmed by calculating the boundaries of the tongue by numerically solving the values for which the two critical points are directly mapped onto each other, and the values for which the symmetric orbit occurs, by determining for which values $z_{\max}$ and $z_{\min}$ are mapped onto each other by a single application of the map. These special trajectories are known to form the boundaries of the period two window for each value of ε from Section 4.

7. Discussion

This study shows that smooth convex geometries bear the possibility of wave attractors. Even small (smooth) perturbations to the circle can lead to wave attractors, with an Arnol'd tongue with an opening that is linear in ε, provided that the perturbation can be described in Fourier components of period 4 or higher. So no singularities like corners or critical latitude singularities are needed. But for such period 4 perturbations it becomes hard to investigate the parameter space analytically, as expressions for ray tracing become difficult to handle.

For the third degree curve, the attractor only appears in the second order in the perturbation theory. But for this curve the expressions needed for ray tracing are easily obtained analytically, although when iteration of the map is involved a numerical approach is required. The parameter space was investigated in detail to study the structure of the windows with attractors and the role of symmetry. Windows containing an attracting periodic orbit are bounded by parameter values that imply either periodic orbits connecting critical points, or imply a 'merging' of two attractors of the same period, that are each other's mirror image with respect to the z-axis in the rest of the window, resulting in a single z-symmetric attractor. The periodic orbits belonging to the boundary of a window are only weakly attracting, the Lyapunov exponent vanishes. A single standing mode is detected, present for all values of ε and owing its existence to an additional symmetry of the system for this specific value of κ. This standing mode disappears when this symmetry is destroyed by rotation of the curve. Then the mirror-symmetry with respect to the z-axis is also broken, resulting in a different ordering of the windows regarding the period of the attractor.

For inertial waves in the spherical shell, windows with periodic orbits (attractors) are bounded by characteristics that touch the inner or outer sphere at the critical latitude [16]. The strength of these attractors was determined [11].

The Lyapunov exponent either vanishes or becomes $-\infty$ at the boundary of a window. It equals zero (only algebraic convergence) when the characteristic goes from the equator or pole of one sphere to the equator or pole of the other sphere, or to the critical latitude of the outer sphere. When the equator or the pole is part of the attractor, the attractor is symmetric with respect to the equator or the rotation axis, and will also be accompanied by the 'merging' of two attractors. When the characteristic reflects at the critical latitude of the inner sphere $\lambda = -\infty$.

Also the structure of the parameter space of the parabolic basin with a horizontal surface [5] can be described by inspecting special characteristics. Windows of z-symmetric attractors are bounded by parameter values for which the corner is mapped to the other corner of the basin and values for which the two critical points are mapped onto each other. The windows with asymmetric attractors are bounded by values for which a corner and a critical point are mapped onto each other and by values for which the two asymmetric attractors come together in a single symmetric attractor. This is analogous to the third degree curve, where the corners are replaced by critical points.

For the bucket [5] the situation is different. The bucket is a trapezoid with flat top and bottom and two sloping walls of opposite constant slope. Windows with symmetric attractors start with values of κ for which a characteristic joins the two upper corners and end with values of κ for which the two lower corners are mapped onto each other. Therefore reflections at the corners can be interpreted as critical reflections. The asymmetric attractors do not occur because focusing at one side wall is compensated by defocusing at the other side wall. All rays are periodic when this happens (standing mode) and in particular the upper corner is connected to the opposite lower corner.

The 'half bucket' with one sloping wall [18] is closely related. A ray is focused towards a periodic orbit (attractor) that has an odd number of reflections at the sloping wall. When it has an even number of reflections at this wall, a downward, focusing reflection will always be balanced by a defocusing upward reflection so that no net focusing occurs. For the full bucket, focusing on one sloping wall is not compensated at the other sloping wall, but reinforced for a symmetric attractor, since also the sense in which characteristics travel is mirror symmetric. For the half bucket this corresponds to a connection from the upper corner of the sloping wall to the lower corner of the sloping wall. Thus the z-symmetry is not of essential importance for the existence of attractors or standing modes.

When comparing the structure of the variations of the Lyapunov exponent with κ in the different geometries mentioned above, it was noticed that, contrary to the other geometries, for the third degree curve the values of λ varied smoothly. For the parabolic basin this was only the case at the beginning of a window, for the end of the window there was a jump from a finite value of λ to 0. The continuous variation of λ corresponds to the cases where the window is bounded by κ-values for which the true critical points are mapped onto each other or the attractor becomes symmetric, the jump corresponds to the boundary where the corner points are connected to each other or to a critical point. For the bucket-shaped basin, indeed, both boundaries of the window are characterized by a jump in λ. This indicates the singular nature of these corner points.

Acknowledgements

AM was supported by the Dutch organisation for Scientific Research NWO (project number 620-61-392).

Appendix A. Lyapunov exponent

The distance between two parallel characteristics is not uniquely determined in terms of the periodic coordinate ϕ; it depends on which of the two sets of intersection points is chosen. This is illustrated in Fig. 18(a), where $\mathrm{d}\phi_1 < \mathrm{d}\phi_2$. The distance along the curve between the two parallel characteristics has the same problem. This makes these definitions of distance unsuitable to determine the Lyapunov exponent.

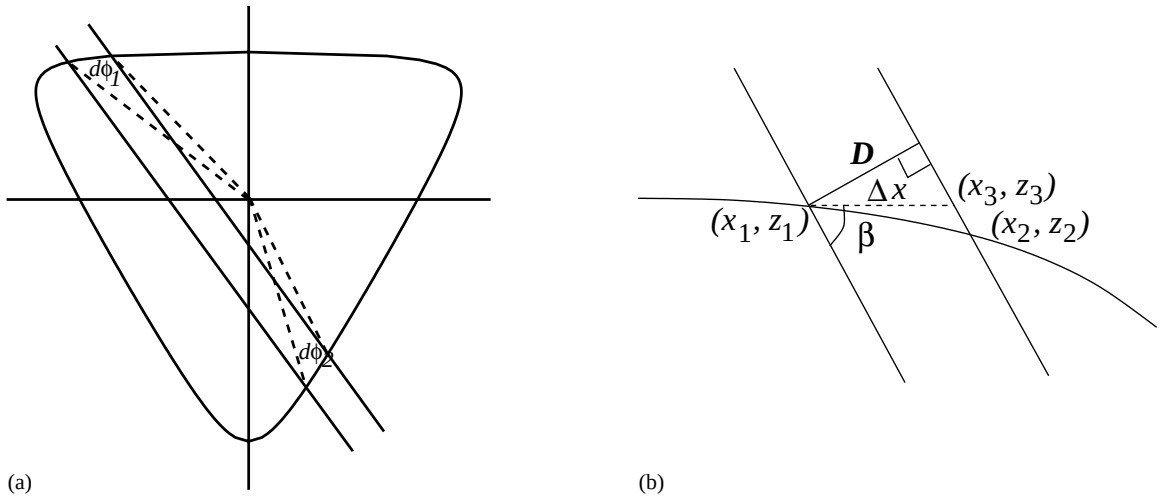

Fig. 18. (a) The angular distance between two rays and the distance along the curve between two rays depends on the precise location of the intersections, here $d\phi_1 < d\phi_2$. (b) Part of the curve with two characteristics to illustrate the definitions in the derivation of the Lyapunov exponent.

Therefore, the perpendicular distance $\mathcal{D}$ between the characteristics is used. This also seems an appropriate choice from a physical viewpoint, where classically a beam of waves, emanating from a generation area is considered, and concentration of energy is related to the beam itself rather than to its contact area with the boundary. The ratio of the distance before and after application of the map T can be used to compute the Lyapunov exponent, as will be shown here.

Fig. 18(b) shows two characteristics, starting on boundary Γ at (x_1, z_1) and (x_2, z_2) and extrapolated outside the boundary. The line connecting (x_1, z_1) and (x_3, z_3) is horizontal, $z_3 = z_1$, the angle β is related to κ via $\beta = \arctan \kappa$. This gives for the perpendicular distance between the characteristics $\mathcal{D}$:

$$\mathcal{D} = \Delta x \sin \beta, \tag{A.1}$$

$$\mathcal{D} = (x_3 - x_1) \sin \beta, \tag{A.2}$$

$$\mathcal{D} = \left(\frac{z_1 - z_2}{-\kappa} + x_2 - x_1 \right) \sin \beta. \tag{A.3}$$

For a given value of z, the x-coordinate of a point on the curve is known from the parameterization of the curve, $x = \mathcal{F}(z)$ up to a sign, that can be found by selecting a specific point on the curve and characteristic to start with, and is taken into account in the computation of $\mathcal{F}$. Substitution leads to

$$\mathcal{D} = \left| \left(\frac{z_1 - z_2}{-\kappa} + \mathcal{F}(z_2) - \mathcal{F}(z_1) \right) \right| \sin \beta. \tag{A.4}$$

The same procedure can be followed to find the distance between the characteristics through the points obtained by iteration of the map T for the points (x_1, z_1) and (x_2, z_2). The new points are denoted by their z-coordinate only, $z_{n+1} = T(z_n)$. The distance after applying the map is denoted by $\mathcal{D}_T$:

$$\mathcal{D}_T = \left| \left(\frac{T(z_1) - T(z_2)}{-\kappa} + \mathcal{F}(T(z_2)) - \mathcal{F}(T(z_1)) \right) \right| \sin \beta. \tag{A.5}$$

The quantity $\mathcal{D}_T/\mathcal{D}$ is closely related to the Lyapunov exponent. If the quantity is larger than 1 the map defocused the two characteristics, if the quantity is smaller than 1 the map focused the characteristics. To derive the definition of the Lyapunov exponent we proceed as follows.

We choose z_2 very close to z_1 so that we can write $z_2 = z_1 + \epsilon$. This results in

$$\frac{\mathcal{D}_T}{\mathcal{D}} = \frac{|((T(z_1) - T(z_1+\epsilon))/-\kappa) + \mathcal{F}(T(z_1+\epsilon)) - \mathcal{F}(T(z_1))|}{|(\epsilon/\kappa) + \mathcal{F}(z_1+\epsilon) - \mathcal{F}(z_1)|}. \tag{A.6}$$

After multiplying numerator and denominator with κ/ϵ and considering the limit $\epsilon \to \infty$ we obtain the formula:

$$\frac{\mathcal{D}_T}{\mathcal{D}} = \frac{|(\mathrm{d}T/\mathrm{d}z)|_{z_1} - \kappa(\mathrm{d}\mathcal{F}/\mathrm{d}z)|_{T(z_1)}(\mathrm{d}T/\mathrm{d}z)|_{z_1}|}{|1 - \kappa(\mathrm{d}\mathcal{F}/\mathrm{d}z)|_{z_1}|}. \tag{A.7}$$

If we apply this formula on and on for the successive iterations of the map T this gives the total divergence or convergence of the map. The definition of λ as measuring the exponential 'separation' of two adjacent points [27], here translated in terms of the distance between the rays, reads

$$\mathcal{D}\,\mathrm{e}^{N\lambda(z_0)} = \mathcal{D}_{T^N}. \tag{A.8}$$

This can be written as

$$\mathrm{e}^{N\lambda(z_0)} = \frac{\mathcal{D}_{T^N}}{\mathcal{D}_{T^{N-1}}}\frac{\mathcal{D}_{T^{N-1}}}{\mathcal{D}_{T^{N-2}}}\cdots\frac{\mathcal{D}_T}{\mathcal{D}}. \tag{A.9}$$

Note that individual $\mathcal{D}$-terms cannot be eliminated, since an expression for the *ratio* has been obtained (Eq. (A.7)) and individual distances have no meaning. Rewriting and taking the limit $N \to \infty$ yields an analogon for the 'classical' formula for the Lyapunov exponent λ:

$$\lambda(z_0) = \lim_{N\to\infty}\frac{1}{N}\sum_{n=1}^{N-1}\log\frac{\mathcal{D}_{T^n}}{\mathcal{D}_{T^{n-1}}}. \tag{A.10}$$

References

[1] H. Görtler, Über eine Schwingungserscheinung in Flüssigkeiten mit stabiler Dichteschichtung, Z. Angew. Math. Mech. 23 (1943) 65–71.
[2] H. Görtler, Einige Bemerkungen über Strömungen in rotierenden Flüssigkeiten, Z. Angew. Math. Mech. 25 (1944) 210–214.
[3] E. Høiland, Discussion of a hyperbolic equation relating to inertia and gravitational fluid oscillations, Geophys. Publ. 12 (XXIV) (1962) 211–227.
[4] J.N. Franklin, Axisymmetric inertial oscillations of a rotating fluid, J. Math. Anal. Appl. 39 (1972) 742–760.
[5] L.R.M. Maas, F.-P.A. Lam, Geometric focusing of internal waves, J. Fluid Mech. 300 (1995) 1–41.
[6] M.E. Cartan, Sur les petites oscillations d'une masse de fluide, Bull. Sci. Math. 46 (1922) 317–369.
[7] C. Wunsch, Progressive internal waves on slopes, J. Fluid Mech. 35 (1969) 131–144.
[8] D. Cacchione, C. Wunsch, Experimental study of internal waves over a slope, J. Fluid Mech. 66 (1974) 223–239.
[9] H.P. Greenspan, On the inviscid theory of rotating fluids, Stud. Appl. Math. 48 (1968) 19–28.
[10] R.C. Beardsley, An experimental study of inertial waves in a closed cone, Stud. Appl. Math. 49 (1970) 187–196.
[11] M. Rieutord, B. Georgeot, L. Valdettaro, Inertial waves in a rotating spherical shell: attractors and asymptotic spectrum, J. Fluid Mech. 435 (2001) 103–144.
[12] M.E. Stern, Trapping of low frequency oscillations in an equatorial 'boundary layer', Tellus XV (3) (1963) 246–250.
[13] P. Bretherton, Low frequency oscillations trapped near the equator, Tellus XVI (2) (1964) 181–185.
[14] K. Stewartson, On trapped oscillations of a rotating fluid in a thin spherical shell, Tellus XXII (6) (1971) 506–510.
[15] K. Stewartson, On trapped oscillations of a rotating fluid in a thin spherical shell II, Tellus XXIV (4) (1972) 283–286.
[16] M. Israeli, On trapped oscillations of rotating fluids in spherical shells, Stud. Appl. Math. 51 (1972) 219–237.
[17] F. John, The Dirichlet problem for a hyperbolic equation, Am. J. Math. 63 (1941) 141–154.
[18] L.R.M. Maas, D. Benielli, J. Sommeria, F.-P.A. Lam, Observation of an internal wave attractor in a confined, stably stratified fluid, Nature 388 (1997) 557–561.

[19] L.R.M. Maas, Wave focusing and ensuing mean flow due to symmetry breaking in rotating fluids, J. Fluid Mech. 437 (2001) 13–28.
[20] A.M.M. Manders, L.R.M. Maas, Observations of inertial waves in a rectangular basin with one sloping boundary, J. Fluid Mech., in press.
[21] A. Tilgner, Driven inertial oscillations in spherical shells, Phys. Rev. E 59 (1999) 1789–1794.
[22] W. Krauss, Interne Wellen, Gebr. Borntraeger, Berlin, 1966.
[23] I. Tolstoy, Wave Propagation, McGraw-Hill, New York, 1973.
[24] V.I. Arnol'd, Small denominators. I. Mappings of the circumference to itself, Am. Math. Soc. Transl., Ser. 2 46 (1965) 213–263.
[25] W. De Melo, S. van Strien, One-dimensional Dynamics, Springer, Berlin, 1993.
[26] E.A. Coddington, N. Levinson, Theory of Ordinary Differential Equations, McGraw-Hill, New York, 1955.
[27] H.G. Schuster, Deterministic Chaos, Physik Verlag, 1984.
[28] W.W. Wood, Properties of inviscid, recirculating flows, J. Fluid Mech. 22 (1965) 337–346.
[29] P.G. Baines, Forced oscillations of an enclosed rotating fluid, J. Fluid Mech. 30 (1967) 533–546.
[30] A.D. McEwan, Inertial oscillations in a rotating fluid cylinder, J. Fluid Mech. 40 (1970) 603–640.